4
Experimentation

4.1 Materials

The elemental composition of various minerals used to prepare electrode coatings is shown in Table 4.1. Table 4.2 represents the chemical composition of the base materials joined and respective filler wires used for joining. The elemental composition of minerals was obtained using XRF technique. Due to the limitation of XRF apparatus used in this study O and F content could not be detected experimentally.

Table 4.1: Chemical composition of various minerals (wt.%)

Mineral (source)	Chemical composition (wt.%)						
	Ca	Ti	Al	Fe	Si	S	Mg
Rutile (TiO_2)	-	87.462	5.945	1.578	4.092	0.297	-
Calcite (CaO)	81.451	-	4.619	0.742	2.954	-	9.481
Silica (SiO_2)	0.483	-	2.822	0.174	96.161	0.293	-
Fluorspar (CaF_2)	92.771	-	4.976	0.413	1.388	-	-
Calcinated Bauxite (Al_2O_3)	4.086	-	83.021	0.381	1.283	-	-

Table 4.2: Elemental composition of base materials (B) and core wire (F) (wt. %)

Material	Elements (wt.%)										
	C	Si	Mn	P	S	Cr	Mo	Ni	Nb	Ti	Fe
P22 (B)	0.05	0.19	0.42	0.012	0.007	2.32	1.08	-	-	-	Bal.
P91 (B)	0.09	0.24	0.37	0.007	0.002	8.67	0.91	0.11	-	-	Bal.
SS304L (B)	0.025	0.5	1.6	0.045	0.005	18.2	-	8.5	-	-	Bal
ER90S-B3 (F)	0.10	0.48	0.61	0.009	0.006	2.52	1.08	0.10	-	-	Bal.
IN-82 (F)	0.013	0.11	3.16	0.005	0.002	20.2	0.91	72.8	2.62	0.37	0.43

The shielded metal arc welding electrodes were designed and developed based on CaO-CaF_2-SiO_2 and CaO-SiO_2-Al_2O_3 systems. The rutile (TiO_2) as an additional ingredient was added to improve the slag detachability and arc stability of the welding electrodes.

4.2 Extreme vertices design (Design of Experiment)

The coating formulations of welding electrodes were designed using extreme vertices design as suggested by previous authors (Cornell, 2002; Mclean & Anderson, 1966). The method suggests that constraint mixture design for a mixture of k ingredients having both lower and upper bounds on some or all of the ingredients may be represented mathematically as follows (Eq. 4.1 and 4.2):

$0 \le \alpha_i \le x_i \le \beta_i \le 100$ (4.1)

and

$\sum_{i=1}^{n} x_i = 100$ (4.2)

In the above equations, *i=1, 2, 3... n*; a_i and β_i are the upper and lower limits of constraints on the x_i, which is the percentage composition of i^{th} ingredient in the mixture.

When there are no lower and upper bounds on the ingredients of a mixture, the geometric description of the confined design space is easy to define and consists of all points on or inside the boundaries of a regular (k-1)-dimensional simplex. So, the experimental mixture design space of k dimensions is reduced to a (k-1) dimensional simplex.

For three-ingredient mixture system (k=3), the three-dimensional design space (cube) is reduced to a two-dimensional simplex (equilateral triangle), and for k = 4, it is a tetrahedron, as shown in Figures 4.1 and 4.2, respectively.

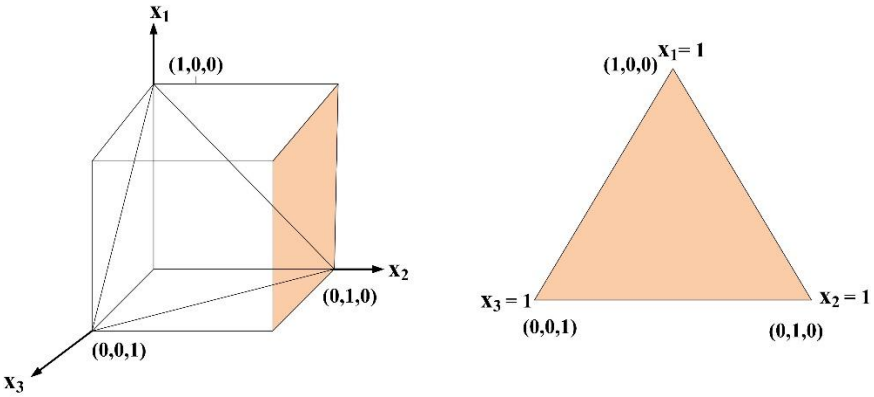

Figure 4.1: Three ingredient simplex design space (Cornell, 2002)

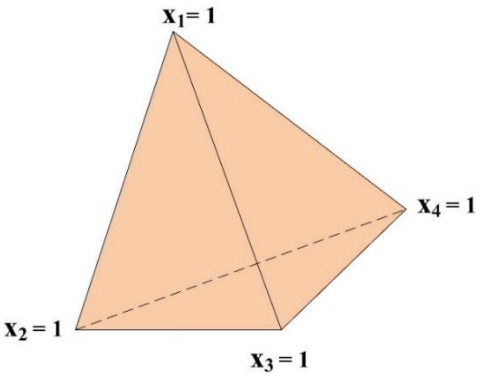

Figure 4.2: Four component tetrahedron (Cornell, 2002)

The confined design space is also not so difficult to define even when only one or two ingredients of the mixture are restricted. It takes the form of hyper-polyhedron or convex polyhedron for the mixture having a greater number of constraints with both lower as well as upper bounds.

To model the response surface of measured properties over the polyhedron region (confined design space) defined by Eq. 4.1 and 4.2, the various design points are specified. The design points represent the various vertices and centroids of the faces of the polyhedron. To obtain the vertices of the polyhedron first of all, the possible combinations (as in two-level factorial method) of proportions of (k-1) ingredients using their lower and upper bound limits are listed. The proportions of the one ingredient are left blank. This procedure produces 2^{k-1} points. The same process is repeated for all the ingredients by keeping alternatively the proportions of one ingredient blank in the list. It will generate a total list of $k.2^{k-1}$ possible combinations. The proportions of the left-out ingredients in the list are specified in a manner satisfying their lower and upper bound limits as well as the condition that the sum of all ingredients must be 100% or unity. In this way, the vertices of the polyhedron are obtained. In the next step, the centroids of the various two-dimensional faces are found by grouping the vertices of the polyhedron. The overall centroid of the polyhedron is obtained by averaging all the vertices of the polyhedron. These design points comprise the complete design matrix for experimentation. The observations of output responses are obtained from which the estimates of the input parameter in the standard mixture design regression models can be calculated.

The output response characteristics for a mixture with k ingredients can be given in the form of a second order regression model as (Eq. 4.3):

$$\mathbf{Y} = \sum_{i=1}^{k} \boldsymbol{b}_i x_i + \sum_{i<j} \sum^{k} \boldsymbol{b}_{ij} \mathbf{x_i x_j} \qquad (4.3)$$

Here, b_i and b_{ij} represents least-square model regression coefficients. The terms $b_i x_i$ and $b_{ij} x_i x_j$ are the individual and interaction effects of the various ingredients of electrode coating, respectively. This type of regression models are without intercept terms and classic terms such as x_1^2 and are known as Scheffe type models.

4.3 Design of welding electrode coatings

The melting point of the coating plays an essential role in the electrode coating design. The electrode coating should melt before the core wire and base metal and remain in the molten state even during the solidification of the weld. The selection of minerals and their composition is generally decided by considering the composite melting point of the coating, which should always be lower than the core wire. Ternary phase diagrams represent the projection of the liquidus surface of the three-component system. Two ternary phase diagrams CaO-CaF_2-SiO_2 and CaO-SiO_2-Al_2O_3 flux systems were used to design the electrode coating for power plant boiler applications (Figure 4.3). The developed coatings are highly basic and having the ability to produce low oxygen as well as low hydrogen content welds. This results in better mechanical properties at higher temperature service conditions. The melting points of the core wire and base metal were approximately in range of 1400-1500°C. Considering the melting point of materials, the composite melting point near to 1100°C-1300°C in the ternary phase diagrams was selected (encircled area) to decide the composition range of CaO, CaF_2, SiO_2, and Al_2O_3 electrode coating ingredients.

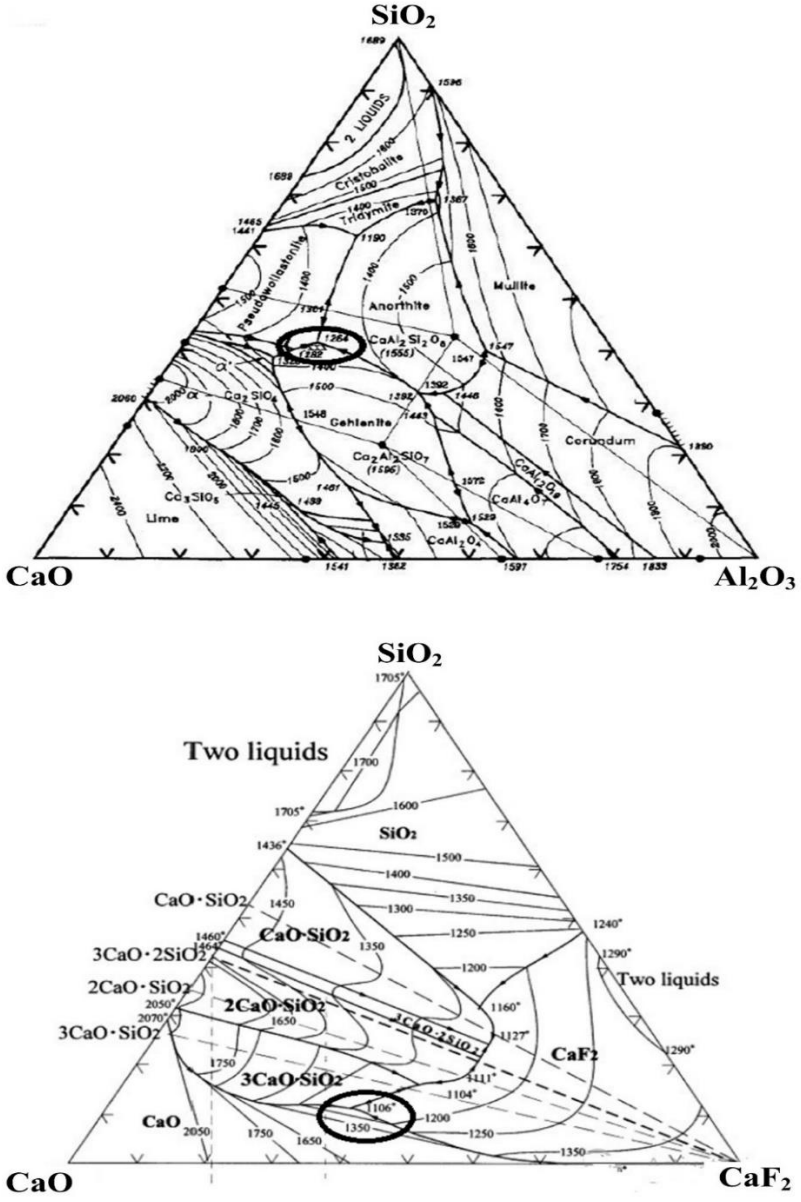

Figure 4.3: Experimental Ternary phase diagrams [Kalisz et al. 2013; Erikson et al. 1993]

The composition of minerals in the coating was fixed as 75% by weight (Eq.4.4 and Eq. 4.5). The remaining 25% composition includes potassium silicate (10% by wt.) and rutile (15% by wt.). These additions were made to improve the slag detachability and arc stability.

$$\left.\begin{array}{l} 20 \leq CaO \leq 25 \\ 35 \leq CaF_2 \leq 40 \\ 05 \leq SiO_2 \leq 10 \\ 01 \leq Al_2O_3 \leq 05 \end{array}\right\} \quad 4.4)$$

$$\sum_{i=1}^{4} x_i = 75 \quad 4.5)$$

Table 4.3 represents the design matrix for electrode coating formulation. The three-dimensional space diagram for the design mixture is shown in Figure 4.4. The space diagram has six vertices, nine-edge centres, five plane centres, and one overall centroid.

Table 4.3: Design Matrix of electrode coating formulations

No.	Point	Coating ingredients				Basicity Index (B.I)
		CaO	CaF_2	SiO_2	Al_2O_3	
C1.	V	25.0	39.5	9.5	1.0	3.36
C2.	V	22.5	37.5	10.0	5.0	2.74
C3.	V	25.0	38.5	8.5	3.0	3.27
C4.	V	24.0	39.0	9.0	3.0	3.23
C5.	V	25.0	40.0	7.0	3.0	3.59
C6.	V	25.0	40.0	5.0	5.0	3.75
C7.	EC	20.0	40.0	10.0	5.0	2.72
C8.	EC	24.6	39.6	9.6	1.0	3.3
C9.	EC	24.5	40.0	9.5	1.0	3.34
C10.	EC	24.5	39.5	10.0	1.0	3.23
C11.	EC	24.0	40.0	10.0	1.0	3.23
C12.	EC	23.3	38.3	8.3	5.0	3.02
C13.	EC	25.0	39.0	10.0	1.0	3.24
C14.	EC	25.0	40.0	9.0	1.0	3.45
C15.	EC	22.5	40.0	7.5	5.0	3.18
C16.	PC	22.0	40.0	10.0	3.0	2.96
C17.	PC	25.0	37.0	10.0	3.0	2.98
C18.	PC	25.0	35.0	10.0	5.0	2.75
C19.	PC	23.5	38.5	10.0	3.0	2.97
C20.	PC	25.0	37.5	7.5	5.0	3
C21.	OC	23.5	40.0	8.5	3.0	3.44

Note: V - Vertex, EC- Edge Centre, PC- Plane Centre, OC- Overall Centroid

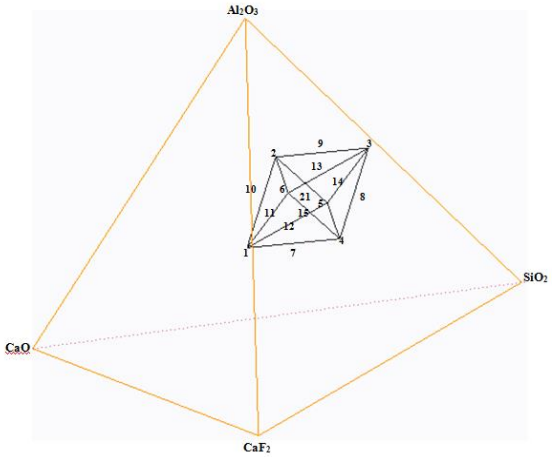

Figure 4.4: Confined design space within the tetrahedron

4.4 Experimentation

4.4.1 Electrode coating preparation

Calcite, fluorspar, silica, calcinated bauxite, and rutile minerals were weighed using a digital weighing balance as per the design matrix present in Table 4.3. After weighing, each mineral was added to the mixer and blended for 15 minutes to prepare a dry mix. The dry mix was placed in the muller, and potassium silicate (act as a binder) was added to the dry mix. The mixture was mixed for 30 minutes in the muller to prepare a wet mix. The prepared wet mixture was left for 24h to dry at room temperature. After drying for 24 hours at room temperature, the coating mixture was baked in an electric oven at 160°C for 2 hours.

4.4.2 Physicochemical and Thermophysical characterization of electrode coatings

The baked coating mixture was crushed into a fine powder to perform physicochemical and thermophysical characterizations. The physicochemical and thermophysical properties like density, thermal conductivity, thermal diffusivity, specific heat, thermal stability, change in enthalpy, wettability behavior of electrode coatings have a significant effect on the fabricated welds. The measurement techniques and experimental setups to investigate these properties are given below.

4.4.2.1 Density

Density was measured using the bulk density method (mass/volume) for electrode coatings at room temperature. A 10ml cylindrical flask was taken and filled completely with crushed electrode coating, which represents the volume of the coating mixture. The weight of the electrode coating contained in the cylindrical flask was measured on an electronic weighing balance. This procedure was repeated 3 times, and the average value is reported.

4.4.2.2 Thermal properties (Weight loss, change in enthalpy, thermal conductivity, thermal diffusivity and specific heat)

The thermogravimetric analysis (TGA) apparatus also referred as simultaneous thermal analyzer (STA) was used to find the thermal stability of electrode coatings by evaluating percentage weight change at the high temperature. Here, the Perkin Elmer simultaneous thermal analyzer 6000 (STA 6000) was used for required experiments. The instrument is equipped with a top-loaded furnace, where temperature can be varied from 15 °C to 900°C at different heating scan rates from 0.1 to 100°C/min with a sample capacity of ~ 1500 mg. The specific thermal properties: conductivity, diffusivity and specific heat were measured using hot-disc apparatus.

4.4.2.3 High temperature wettability properties measurements

A 50 g mixture was prepared for each coating composition by adding different minerals (wt.%) presented in Table 4.3. This dry mixture was taken into a mortar and crushed with the help of pestle for 10-15 minutes. It is essential to mix and crush the minerals well to prepare a uniform powder mix. After mixing, potassium silicate was added to prepare a wet mix. This wet mix was placed in a die and subjected to a pressure of 200 kg/cm^2 in a hydraulic press. A pallet in the dimensions of diameter 10 mm and a height of 13 mm was obtained. The prepared pellets were air-dried for 24 hours and then baked in an oven at a temperature of 160°C for 3 hours (Figure 4.5).

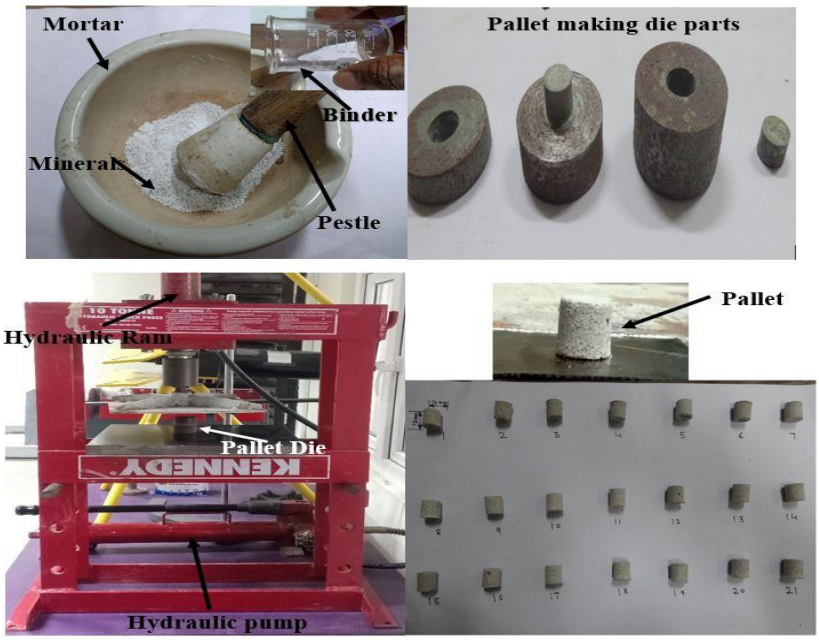

Figure 4.5: Procedure to prepare pallets for twenty-one coating compositions

A sheet of SS304L having a dimension of 50 x 50 x 2 mm was used to investigate the wettability behavior of laboratory-developed coatings. The test temperature parameter was kept at 1150°C. Pallets were placed at the center of the SS304L specimen and placed into the furnace, which was set at a temperature of 1150°C for 120 seconds-The step-wise procedure to heat the different coating composition pallets is presented in Figure 4.6(a-c).

The coating composition pallet was assumed to be a part of a sphere in this analysis. The images of melted pallet were clicked from the front and top using a digital camera. The molten spread area boundary was marked, as shown in Figure 4.6b. Open-source Image-J software was used to measure the spread area and contact angle (Kingery et al., 1953; Kim et al., 2015; Joshi et al., 2017). Figure 4.6c shows the different contact angles estimated for developed coatings.

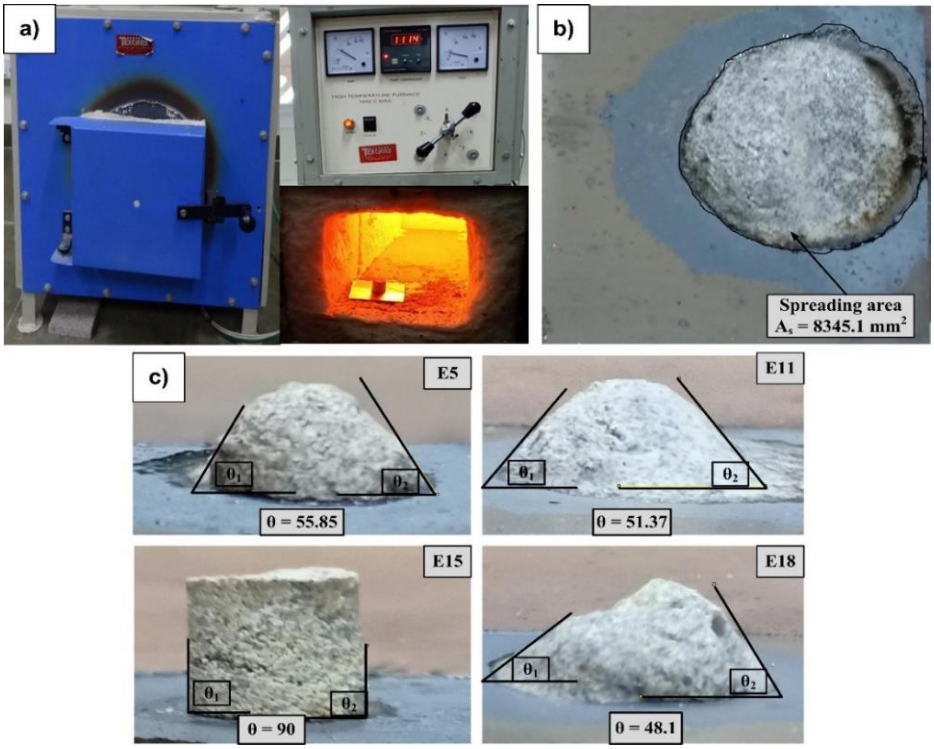

Figure 4.6: Estimation of contact angle and spreading area a) Pallet melting in a furnace b) Spreading area of E11 c) Contact angle measurement for different electrode compositions

Contact angles for all the coating compositions were measured and to describe the correlation between surface & interfacial tensions at various phase boundaries of a liquid drop at equilibrium on solid surface Young's equation was used, as expressed by Eq. 4.6 and Figure 4.7 (Kingery et al., 1953; Shigeta et al., 1989; Yanhui et al., 2014; Kim et al., 2015; Joshi et al., 2017).

$$\gamma_{SL} = \gamma_{SG} + \gamma_{LG} \cos\theta \quad (4.6)$$

where θ is the contact angle; γ_{LS} & γ_{SG} are the interfacial tensions (mN/m) at the solid-liquid and solid-gas interfaces respectively, while γ_{LG} is a molten slag surface tension.

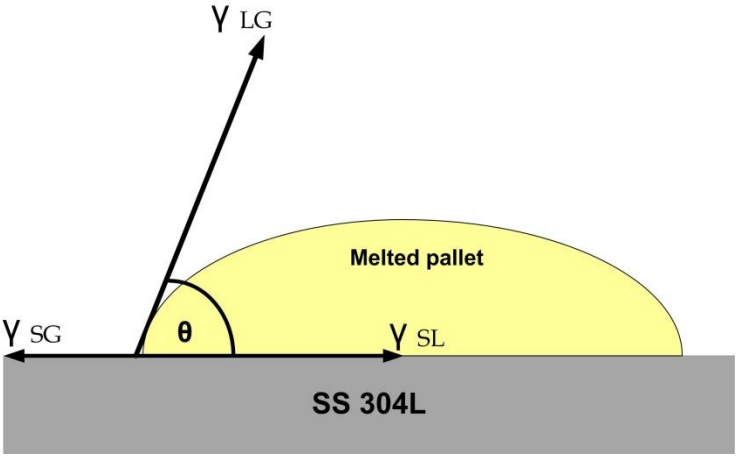

Figure 4.7: Contact angle measurement

Using Boni's empirical equation (Eq. 4.7), γ_{LG} can be calculated (Kim et al., 2015):

$$\gamma_{LG} = x_1 f_1 + x_2 f_2 + x_3 f_3 + \ldots\ldots\ldots\ldots\ldots x_t f_t \quad (4.7)$$

Where γ_{LG} = surface tension in milli-Newtons per meter (mN/m), x_t= percentage mole fraction of a component t (%), and f_t = surface tension factor for different minerals in mN/m. Surface tension factors for pure oxides are presented in Table 4.4: (Kingery et al., 1953; Shigeta et al., 1989; Yanhui et al., 2014; Kim et al., 2015; Joshi et al., 2017).

Table 4.4: Temperature dependence of surface tension of minerals

Oxide	Temperature (K) dependence of surface tension (mN/m)
CaO	791-0.0935*T
CaF_2	407.75-0.07*T
SiO_2	243.2+0.031*T
Al_2O_3	1024-0.177*T
TiO_2	1384.3-0.6254*T

By using surface tension factor and melting temperature, the corresponding surface tension values were calculated for developed coating compositions**.** The wetting behavior of a molten liquid phase with other immiscible phases is indirectly related to the interfacial attribute, i.e., adhesion energy (W_a). It should be inversely proportional to the measured contact angle between molten metal and a solid oxide substrate. The amount of energy per unit area required for removing the contacting material from the heating plate or substrate is known as the adhesion energy. Thus, contact angle should behave opposite to that of adhesion energy because the interfacial area and resistance tend to increase if there is better contact (or lower contact angle) between liquid and solid substrate interface. Using Dupre-Young equation (Eq. 4.8), the adhesion energy can be calculated (Joshi et al., 2017):

$$W_a = \gamma_{LG} * (1 + \cos\theta) \quad (4.8)$$

4.4.3 Structural characterization

After the design and development of electrode coatings, the phase and structural analysis of these coatings need to be investigated. In the present study, X-ray diffraction (XRD) and Fourier transform infrared (FTIR) spectroscopy was used to identify the phases/types of bonds present in different electrode coatings. X-ray diffraction techniques are based on wave interference. It can extract the information of inter-planar spacing using Bragg`s law ($n\lambda = 2d \sin\theta$). The D8 Advance Powder X-ray diffractometer in conjunction with parallel beam geometry was used to identify the various oxide phases present. FTIR has extensively been used for vibrational spectroscopic measurements. It depends on the interaction of infrared radiation with the vibrating dipole moments of molecules. Bruker FTIR spectrometer vertex 70 V was used to observe the structural behavior of developed coatings. This spectrometer consists of a room temperature Deuterated and L-alanine doped Triglycine sulfate (DLaTGS) detector. The resolution of the used FTIR spectrophotometer is ~ 0.4 cm^{-1}.

4.4.4 Manufacturing of coated electrodes

Welding electrodes were manufactured in the electrode manufacturing pilot plant of Weld Alloy Pvt. Ltd., Noida. The electrode manufacturing plant and its working is shown in Figure 4.8. In this study, twenty-one sets of welding electrodes were manufactured. The wet mix was prepared as explained in the section 4.4.1. The core wires of length 350 mm and diameter 3.15 mm were placed in a wire feeder. The prepared wet mix was fed into the cylindrical barrel of a hydraulic press. The flux coating was extruded on the core wires using this setup. The electrodes were checked for eccentricity with the concentric tester. After evaluating all the desired parameters, the manufactured electrodes were kept at room temperature for 24-hour air drying and then baked in an oven at 160°C for 2-hours.

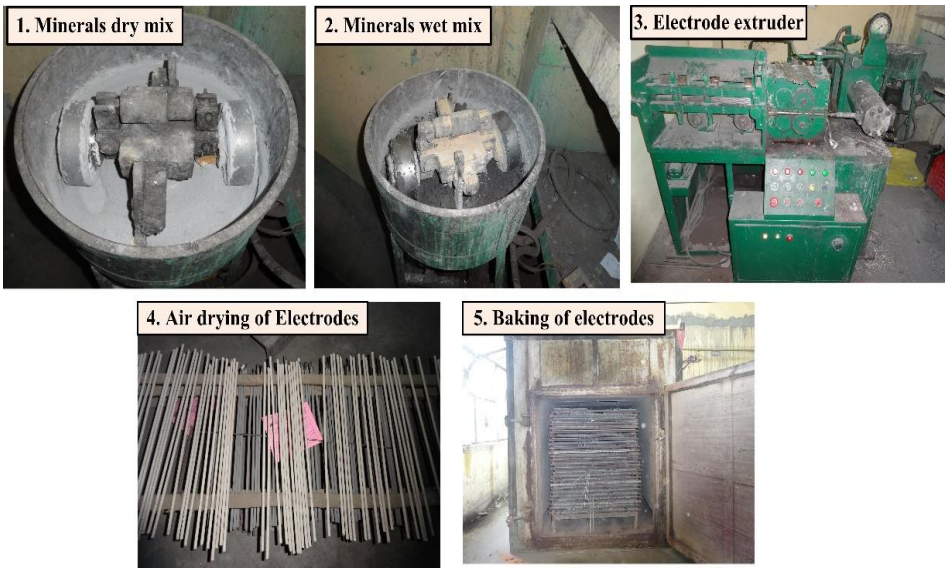

Figure 4.8: Welding electrode extruder setup

4.4.5 Welding parameter selection

The welding parameters play an essential role in influencing the weld quality and performance. It is important to ensure adequate filling with minimum defects. A welding arc is expected to be easily ignitable and remaining stable throughout the weld run with minimum spatter. Several trials were performed to finalize the final arc current. Multipass beads were deposited on the base plate with different welding currents at a constant speed of 2mm/s. The qualitative observation of bead deposited using ER90S-B3 core (purchased from ESAB with standard name TIGROD ER90S-B3) wire-based electrodes at different welding current is summarized in Table 4.5. A current of 100A was found to produce beads with a superior profile, improved slag detachability with better arc stability amongst all. A similar procedure was repeated to finalize

the welding current for nickel-based (IN-82) electrodes (Table 4.6). A current of 90A were selected for IN-82 based electrodes.

Table 4.5: Qualitative observations of ER90S-B3 core wire based laboratory developed electrodes

Current (A)	Bead Appearance	Arc stability	Slag detachability
80	Poor	Poor	Fair
90	Fair	Fair	Fair
100	Good	Good	Fair
120	Fair	Good	Fair

Table 4.6: Qualitative observations of IN-82 core wire based laboratory developed electrodes

Current (A)	Bead Appearance	Arc stability	Slag detachability
80	Fair	Poor	Poor
90	Good	Good	Fair
100	Fair	Fair	Fair
120	Poor	Poor	Poor

4.4.6 Multipass bead on plate analysis

In this investigation, the aim was to choose 2 best coating compositions out of the developed twenty-one compositions. Twenty-one sets of ER90S-B3 electrodes and IN-82 electrodes were manufactured respectively, as explained in section 4.4.4. The ER90S-B3 core wire-based electrodes were manufactured to join P22 to P91 low alloy steels. The IN-82 core wire-based electrodes were manufactured to join P91 low alloy steel to SS304L austenitic stainless steel. Shielded metal arc welding setup was used to deposit multipass weld beads using twenty-one sets of ER90S-B3 and IN-82 electrodes each. All the 42 deposited beads were analyzed for chemical composition using atomic absorption spectroscopy available at Cosmo Analytic Lab, Noida. During the welding process, qualitative observations like arc stability, bead appearance, slag detachability, smoke, spatter, porosity were also recorded. All the observations are discussed in chapter 5. Microhardness testing was also performed to estimate the Vicker`s microhardness of deposited weld beads. After analyzing the qualitative observations, weld chemistry, and mechanical properties for both the electrode coatings, two sets of electrodes were selected to fabricate the final welds. These final welds were compared with welds fabricated using commercial electrodes.

4.4.7 Preparation of weld coupons and fabrication of dissimilar welds

4.4.7.1 Fabrication of P22/91 dissimilar weld using developed and commercial electrodes

The plates to be welded were cut from P22 and P91 base materials to fabricate the dissimilar welds. The plates were cut into the sizes of 250 x 75 x 20 mm, and edges were machined to 30^0 each. The geometry of the dissimilar weld is shown in Figure 4.9. Three different dissimilar welds of P22/P91 were fabricated using the SMAW process by employing the two sets of laboratory-made electrodes and commercial electrode (E9018-B3). Welds were fabricated in direct current electrode positive (DCEP) polarity with parameters presented in Table 4.7. The initial tacking of base plates was done using the GTAW process. Root pass was applied using GTA welding process. Filler same as the core wire of electrode was used for root pass with welding parameters bepresented in Table 4.7. The tacked plates were initially heated to a temperature of 250°C before the SMAW filling. The fabricated welds were post weld heat-treated for 2 hours at a temperature of 760°C in a controlled environment of muffle furnace.

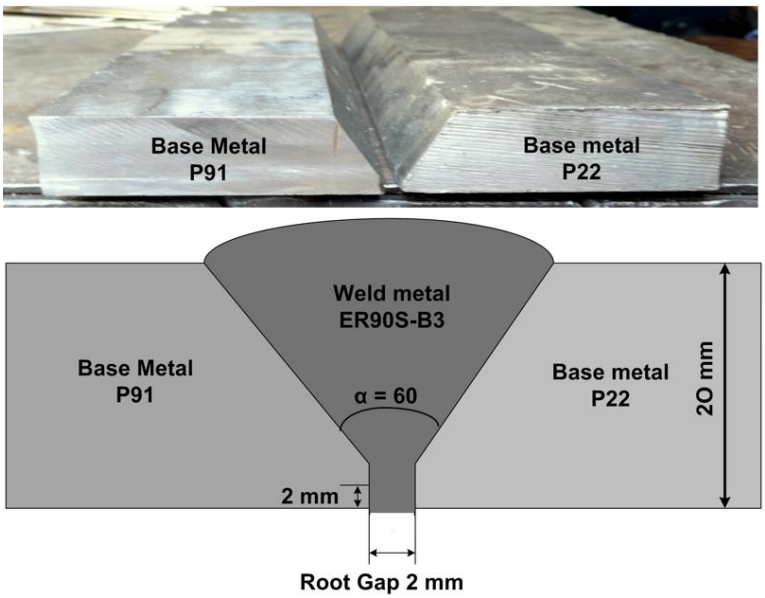

Figure 4.9: Base material plates and weld geometry of P22/P91 dissimilar weld

Table 4.7: Welding parameters

Welding Parameter	P22/P91 GTAW (Root pass)	P22/P91 SMAW (Fill)	P91/SS304L GTAW (Root pass)	P91/SS304L SMAW (Fill)
Current (A)	90	100	90	90
Voltage (V)	15	25	15	25
Speed (mm/sec)	1	2	1	2
Argon Gas flow rate (L/min)	12	-	12	-
Polarity	DCEN	DCEP	DCEN	DCEP

4.4.7.2 Fabrication of P91/SS304L dissimilar weld using laboratory developed and commercial electrodes

The plates to be welded were cut from P91 and SS304L base materials. The plates were cut into the sizes of 250 x 75 x 20 mm, and edges were machined to an angle of 30^0 each (Figure 4.10). Buttering layer of 6mm thickness was applied on P91 with filler wire of IN-82 using GTAW process. The buttered P91 base plate was then heated for 2 hours at a temperature of 750°C in a controlled environment of muffle furnace. The initial tacking of buttered P91 base plate and SS304L base plate was done using the GTAW process. Filler same as the core wire of electrode was used for the buttering and root pass with welding parameters presented in Table 4.7. The Three different dissimilar welds of buttered P91 steel and SS304L steel was fabricated using the SMAW process by employing the two sets of laboratory-developed electrodes (IN-82 based) and one commercial electrode. Welds were fabricated in DCEP polarity with parameters presented in Table 4.7.

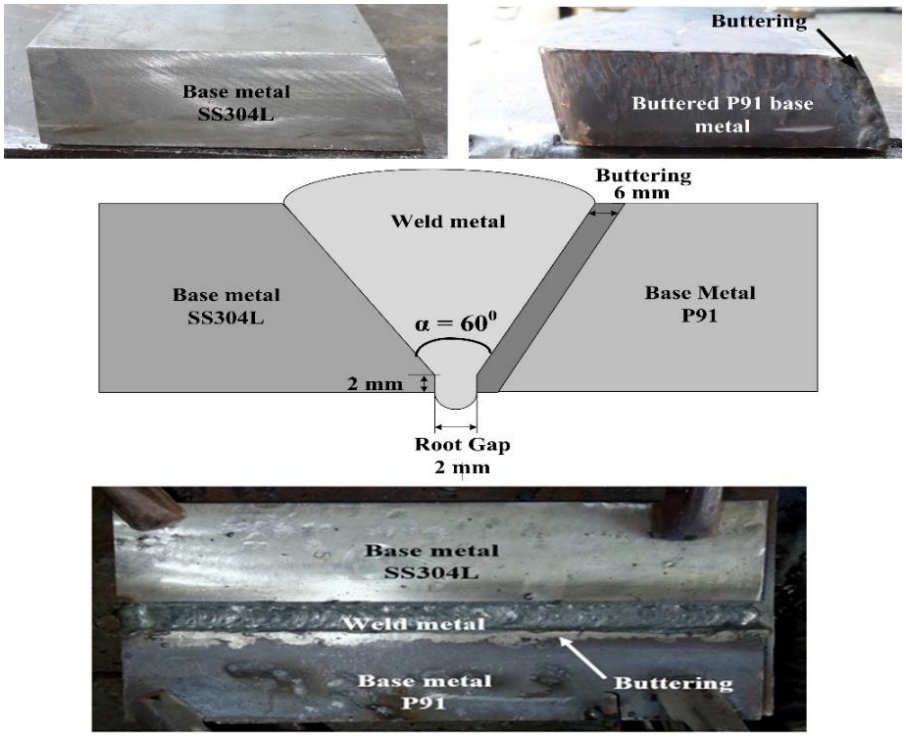

Figure 4.10: Base material plates and weld geometry of P91/SS304L dissimilar weld

4.4.8 Weld characterization

The various characterizations were performed on the fabricated dissimilar welds to evaluate the weld performance. As illustrated in Figure 4.11, specimens were machined from the weldments for various mechanical and metallographic characterizations. Tensile tests on longitudinal and transverse weld specimens were performed as per the ASTM E8M standard.

Universal testing machine (Instron M-5982) was used to perform the tensile tests. To validate the accuracy of tensile test results, three specimens were tested for each set of parameters. Charpy V-notch impact test was also performed as per the ASTM E23-07AE1 standard to estimate the impact toughness of the different welds at room temperature. The specimen for Charpy V-notch impact test is shown in Figure 4.11. Cross-sectional Vickers microhardness measurements were conducted on the welds and base metals of etched specimens at a load of 100 gf, with a dwell time of 10s to obtained hardness profile. Microhardness tester (Model MVH-Sauto) was used to evaluate the microhardness profile of dissimilar welds as per ASTM-E384 standard. The chemical compositions of fabricated welds were estimated using the atomic absorption spectrometer available at Cosmo Analytical Lab, Noida.

The metallographic specimen of weld joint was prepared to study the microstructure of base metals, weld zone and heat-affected zone. Specimens were grinding against the silicon carbide papers starting from grade 80 to 2000, followed by final cloth polishing with alumina paste. Table 4.8 illustrates the different etchants used to etch the specimens.

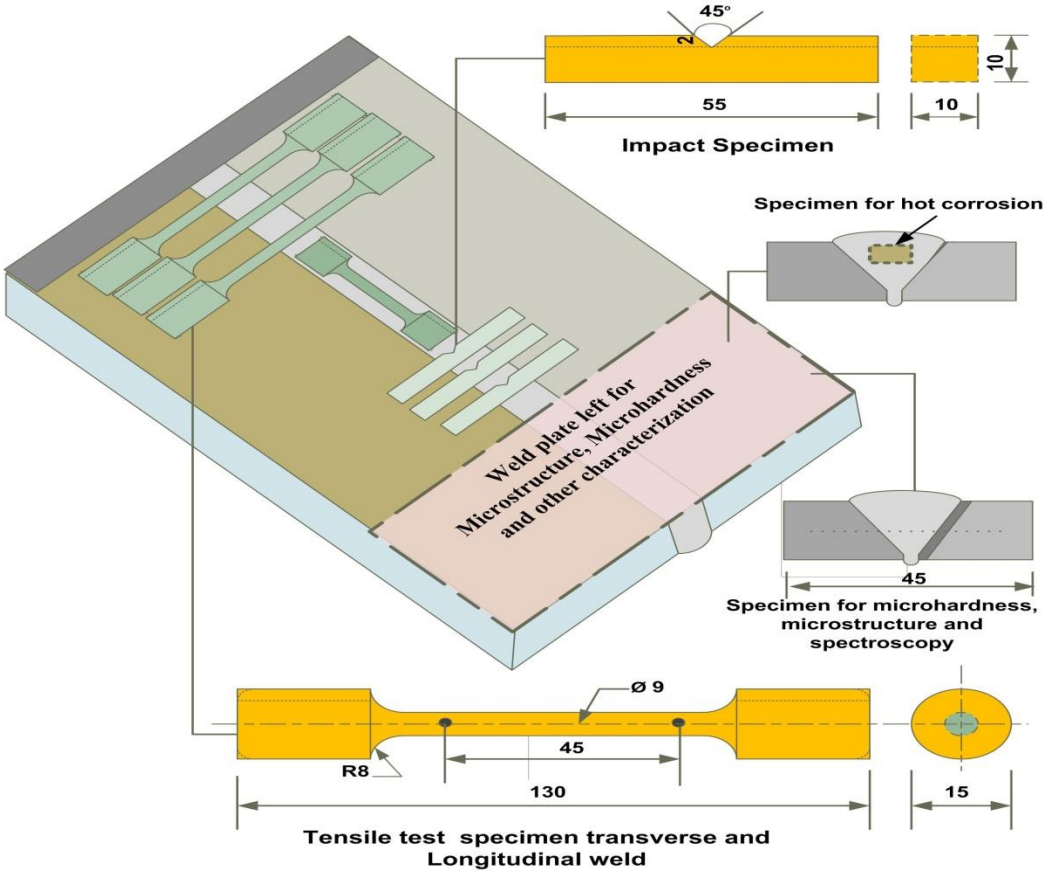

Figure 4.11: Specimen preparation for various characterizations from fabricated dissimilar welds

Table 4.8: Various etchants used to observe microstructure of dissimilar welds

S. No	Region	Etchant	Composition
1	P22 base	Nital 2%	100ml Ethanol + 2ml HNO_3
2	P91 base	Vilella`s Reagent	1g Picric Acid + 5ml HCl + 100ml Ethanol
3	SS304L base	Aqua Regia	15ml HCl + 5ml HNO_3
4	Weld (P22/P91)	Nital 5%	100ml Ethanol + 5ml HNO_3
5	Weld (P91/SS304L)	Electro etch	10% aqueous oxalic acid

4.4.9 Hot corrosion investigations

Hot corrosion studies were conducted on the base materials (P22, P91, SS304L) and fabricated weld specimens. The investigations were performed at a temperature of 650°C, 750°C, and 850°C under the exposure of Na_2SO_4 + 60% V_2O_5 (SM1) and Na_2SO_4 + 50% NaCl (SM2). The specimen was prepared by wire cut EDM (electric discharge machining) in the dimensions of 20mm x 15mm x 5mm. All the faces of specimens were grinding against the silicon carbide papers starting from grade 80 to 2000, followed by final cloth polishing with alumina paste.

The polished specimen was first cleaned with acetone and dried using a hot air gun. Afterward, the specimen was placed in a clean alumina crucible, and the weight of the specimen, along with the crucible, was noted. After measuring the weight, the specimen with the crucible was heated up to 250°C for 1 hour to remove any impurities and moisture. Salt powders were mixed in the desired proportions, and then a few drops of distilled water were added to the salt mixture to make a thick paste. After one hour, the specimen was taken out, and the prepared salt paste was applied to the specimen. The specimen was heated for 3-hours at 110°C in the oven to dry the salt paste. After 3-hours of baking, the specimen was cooled down to the room temperature, followed by the weighing of the specimen along with the crucible. The furnace was set at the desired temperature, and the specimen was placed into the furnace. After 1-hour, the specimen was cooled down to room temperature, and the weight of the specimen along with the crucible was noted. In the hot corrosion experiments, 1 cycle consist of 1-hour heating and 20

minutes cooling and generally referred as 1-hour study. This process is repeated for 50 cycles to perform 50-hours of study. Average values of speciemen weight were taken for the experiments performed on 3 different specimens for all the conditions.

During hot corrosion experimentation, after the completion of each cycle, the weight of the specimen, including crucible, was measured using an electronic weighing balance model Citizen CY 205C with readability 0.01 mg. Weight change measurements included the spalled scale, if any. The specimen was observed visually to note the changes in color and the luster of the oxide scales after the cyclic thermal loading. Bruker D8 Advance Powder X-ray diffractometer, in conjunction with parallel beam geometry, was used to carry out the structural analysis of the different oxide phases present in the corroded specimen. A corroded surface of the specimen was exposed to the X-ray beam during XRD analysis to analyze the different oxide phases present. Before performing the SEM analysis, the specimen was embedded in epoxy and polished using SiC papers up to grade 1000, followed by velvet cloth polishing to attain a mirror polished surface. Carl Zeiss SEM EVO 18 special edition scanning electron microscope with a back-scattered imaging system in conjunction with an energy dispersive spectroscopy (EDS) accessory installed at IIT Jodhpur was used to characterize the surface properties and elemental analysis of the oxide scale formed. SEM/EDS line scan and elemental point analysis were used to analyze the cross-section of different specimens.